

Structural and superconducting properties of $R_{1-x}Ca_xBa_2Cu_3O_{7-\delta}$ with $0.50 \geq x \geq 0.00$

A. Sedky and Anurag Gupta

National Physical Laboratory, K.S. Krishnan Marg, New Delhi 110012, India

V. P. S. Awana

Institute for Superconducting and Electronic Materials, University of Wollongong, New South Wales 2522, Australia

A. V. Narlikar

National Physical Laboratory, K.S. Krishnan Marg, New Delhi 110012, India

(Received 6 May 1998)

We report here a consolidated study of structural and superconducting properties of Ca substituted $R_{1-x}Ca_xBa_2Cu_3O_{7-\delta}$ system, with $R = \text{Er, Y, Sm, and Nd}$, and for $0.50 \geq x \geq 0.00$. Interestingly, with increasing x , Er/Y samples show a behavior significantly different from Sm/Nd. In particular (1) orthorhombic distortion of $R:123$ lattice is found to be little affected for Er/Y samples with increasing x in comparison to Sm/Nd samples, (2) although Ca substitution leads to oxygen depletion for all the four sets of samples, the average Cu valence is, in general, found to remain invariant with x , (3) $\rho(T)$ is found to show an upward curvature for Er/Y samples, which is absent for the Sm/Nd samples, and (4) $T_c(\rho=0)$ as a function of x and δ shows a much steeper decrease in Er/Y based samples, than in Sm/Nd based ones. Our results unequivocally point to a different structural order or disorder in Er/Y samples as compared to Sm/Nd based samples. We suggest that different site preferences of oxygen vacancies, predominantly created in CuO_2 planes (CuO chains) of Er and Y (Sm and Nd) based samples, might be responsible for the observed difference in the behavior. This contention is supported by a host of other considerations and experimental observations. [S0163-1829(98)03942-3]

I. INTRODUCTION

It has been long recognized that aliovalent substitution in high-temperature superconductors (HTSC's), when the substitute has a lower valence, leads to either a decrease in total oxygen content or an increase in average Cu valence or both. One particular case has been that of partial substitution¹⁻¹⁰ of divalent Ca in place of trivalent Y in $Y_{1-x}Ca_xBa_2Cu_3O_{7-\delta}$, that is, the $Y_{1-x}Ca_x:123$ system, which exhibited several interesting features depending on the sample preparation conditions. Essentially, the optimally oxygenated $Y_{1-x}Ca_x:123$ samples were prepared either by the usual procedure of furnace cooling in oxygen or by prolonged slow cooling in oxygen with high partial pressures. In both cases, as x increases from zero to about 0.35 (beyond which the sample is a multiphase), the samples show a gradual decrease in superconducting critical temperature T_c . However, in the former case, a systematic decrease in the oxygen content along with the average Cu valence remaining essentially invariant, and in the latter case, little change in oxygen content along with an increase in average Cu valence has been observed. Interestingly, in the former case, the x-ray diffraction (XRD) data show little or no change in the size and structure of crystallographic unit cell which remains orthorhombic with a -, b -, and c -lattice parameters exhibiting no significant changes with x . These observations led some of us^{5,6} to conclude that with Ca substitution the oxygen depletion was presumably taking place within CuO_2 planes, a fact which was subsequently substantiated by the NMR studies of Kontos *et al.*⁷

The present work, forming a sequel to Refs. 5 and 6, was

carried out in an attempt to test some of the above contentions, including the role of local structural disorder in CuO_2 planes and chains in relation to superconductivity. We have investigated Ca substitution in $R:123$ with $R (= \text{Er, Y, Sm, and Nd})$ of varying ionic sizes. Broadly speaking, if the scenario of carrier concentration change due to $\text{Ca}^{2+}/\text{R}^{3+}$ aliovalence is more important, then the normal state and superconducting properties should be independent of the chosen R , as observed in pure $R:123$ system. However, our results are in variance with this notion, and the present work highlights the contrasting normal state and superconducting properties of Er and Y, with respect to Sm and Nd based Ca substituted samples.

II. EXPERIMENTAL DETAILS

Samples of the series $R_{1-x}Ca_xBa_2Cu_3O_{7-\delta}$ ($R = \text{Er, Y, Sm, and Nd}$), with x ranging from 0.0 to 0.50, were synthesized through a solid state reaction method. The ingredients R_2O_3 , BaCO_3 , CaCO_3 , and CuO of 4N purity were thoroughly mixed in required proportions and calcined at 900 °C in air for a period of 16 h. This exercise was repeated three times with intermediate grinding at each stage. The resulting powders were ground, mixed, pelletized, and annealed in flowing oxygen at 940 °C for a period of 24 h, and then furnace cooled to room temperature with an intervening annealing for 16 h at 600 °C. The samples were characterized for their phase purity by x-ray diffraction. The lattice parameters were determined from a least-square fit of the observed

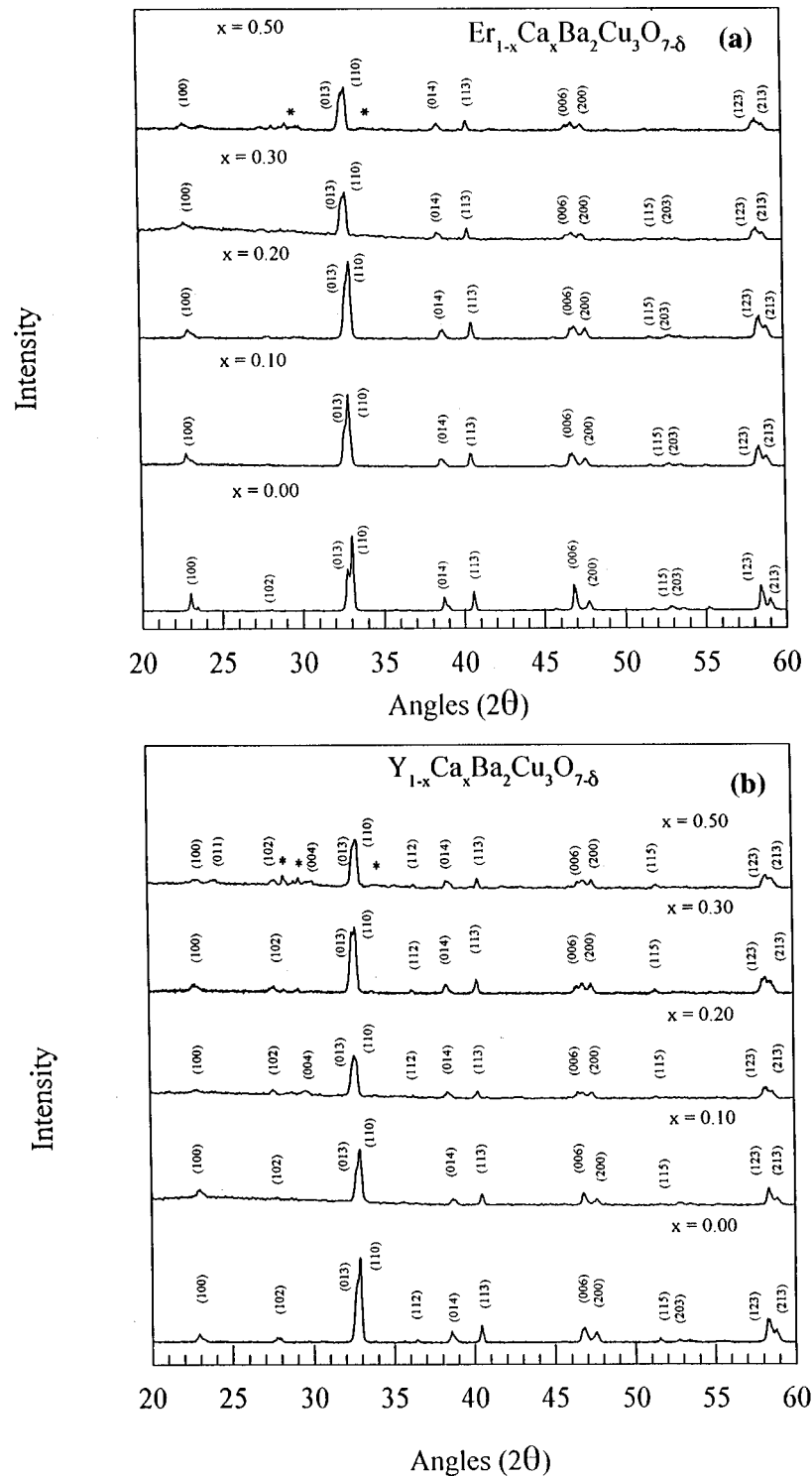


FIG. 1. X-ray diffraction patterns of (a) $\text{Er}_{1-x}\text{Ca}_x\text{Ba}_2\text{Cu}_3\text{O}_{7-\delta}$, (b) $\text{Y}_{1-x}\text{Ca}_x\text{Ba}_2\text{Cu}_3\text{O}_{7-\delta}$, (c) $\text{Sm}_{1-x}\text{Ca}_x\text{Ba}_2\text{Cu}_3\text{O}_{7-\delta}$, and (d) $\text{Nd}_{1-x}\text{Ca}_x\text{Ba}_2\text{Cu}_3\text{O}_{7-\delta}$. The asterisks represent impurity peaks.

d values. The resistivity measurements were obtained in the temperature range of 30–300 K using the four-probe technique in a closed cycle refrigerator. The oxygen content of all the samples was determined by iodometric titration. ac magnetic susceptibility measurements were done in the temperature range of 4.2–300 K, using a Quantum Design SQUID magnetometer, in an applied field of 0.01 mT at 117 Hz.

III. RESULTS

A. X-ray diffraction

Figures 1(a)–1(d) show the room temperature x-ray patterns of $\text{R}_{1-x}\text{Ca}_x\text{Ba}_2\text{Cu}_3\text{O}_{7-\delta}$ ($\text{R}=\text{Er}, \text{Y}, \text{Sm}, \text{and Nd}$ with $x=0.0$ to 0.50) samples. It is evident from these figures that for all the four series Ca substitutes isostructurally in most of the x range. However, a few unidentified low intensity lines

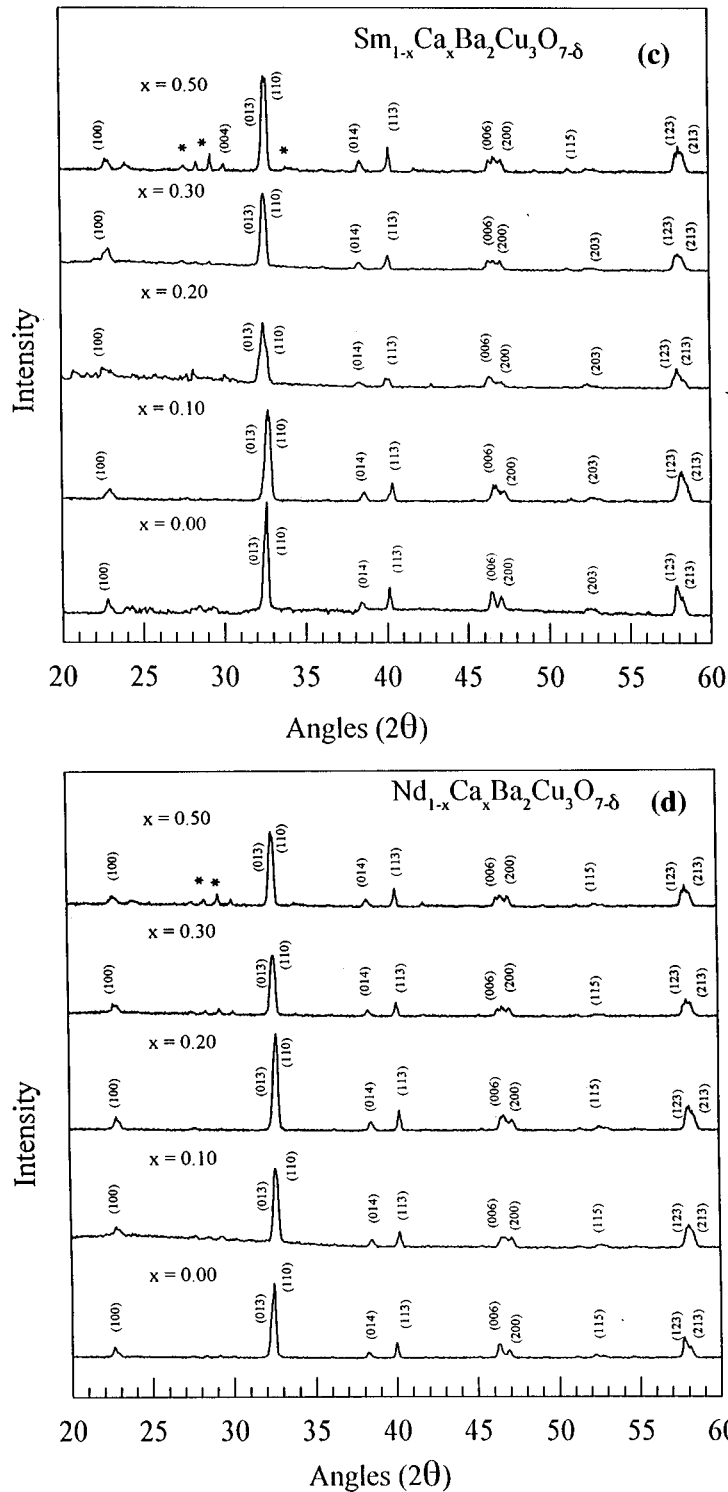


FIG. 1. (Continued).

for $x=0.50$ samples mark the solubility limit of Ca in all the tried $R:123$ systems. In general, the b parameter is found to decrease along with a small increase in the a parameter, resulting in a decreased orthorhombic distortion (OD) [$= (b - a)/b$]. The OD remains nearly invariant until $x=0.30$ for Er and Y samples, and later decreases slightly for $x=0.40$ and 0.50 . The c -lattice parameter for both Er and Y samples increases slightly with Ca doping. Lattice parameters a , b , and c , and the OD are listed in Table I for all the samples of

the Y and Er series. Interestingly, unlike for Er and Y samples, the OD decreases continuously with x for Ca doping in Sm and Nd based samples. The c -lattice parameter of Sm and Nd samples increases with x , which is comparatively more than that observed for Er/Y samples. The lattice parameters for the samples along with their orthorhombic distortion are given in Table I.

A careful survey of the x-ray patterns, e.g., Fig. 1(d) for Nd series further shows formation of orthorhombic II phase.

TABLE I. Lattice parameters a , b , and c , orthorhombic distortion ($b-a/b$), T_c ($\rho=0$), average copper valance (Cu^{p+}), and the total oxygen content ($7-\delta$) for $R_{1-x}\text{Ca}_x\text{Ba}_2\text{Cu}_3\text{O}_{7-\delta}$.

R	x	$a(\text{Å})$	$b(\text{Å})$	$c(\text{Å})$	$(b-a/b)$	T_c ($\rho=0$)	p	$7-\delta$
Er	0.0	3.8163	3.8707	11.6789	0.014	90	2.295	6.943
Er	0.10	3.8109	3.8763	11.6743	0.017	78	2.271	6.856
Er	0.20	3.8193	3.8823	11.6803	0.016	64	2.267	6.800
Er	0.30	3.8207	3.8763	11.6863	0.014	54	2.271	6.756
Er	0.50	3.8293	3.8703	11.6894	0.011	44	2.270	6.655
Y	0.0	3.8195	3.870	11.6777	0.013	90	2.284	6.926
Y	0.10	3.8161	3.8811	11.6852	0.017	78	2.278	6.867
Y	0.20	3.8229	3.8884	11.6826	0.017	67	2.277	6.815
Y	0.30	3.8288	3.8813	11.6923	0.014	55	2.266	6.749
Y	0.50	3.8361	3.8746	11.6951	0.010	46	2.276	6.660
Sm	0.0	3.8247	3.8895	11.7103	0.017	89	2.271	6.906
Sm	0.10	3.8279	3.8802	11.7187	0.014	79	2.258	6.837
Sm	0.20	3.8367	3.8706	11.7234	0.012	73	2.241	6.761
Sm	0.30	3.8401	3.8645	11.7306	0.009	68	2.245	6.720
Sm	0.50	3.8468	3.8601	11.7396	0.008	64	2.248	6.622
Nd	0.0	3.8207	3.8863	11.7059	0.017	88	2.277	6.915
Nd	0.10	3.8263	3.8813	11.7113	0.014	82	2.265	6.848
Nd	0.20	3.8291	3.8763	11.7234	0.008	74	2.261	6.792
Nd	0.30	3.8307	3.8643	11.7297	0.006	71	2.254	6.731
Nd	0.50	3.8317	3.8623	11.7369	0.004	70	2.254	6.630

The double peaks at $2\theta \approx 46.5^\circ$ with increasing x show a clear evolution towards a triplet peak structure, which has been identified¹¹ with the appearance of an ortho II phase. As shown in the next section, the increase of x leads to an increase in oxygen loss (δ) for all the four series of samples (see Table I). For Nd based series, all the three peaks attain the same intensity for $x \geq 0.3$ sample endorsing the formation of the ortho II phase. In contrast, for Er based samples, even though the third peak does make a small appearance for $x \geq 0.3$, the relative intensity of the peaks in the original ($x=0$) doublet diminishes much less [see Fig. 1(a)]. Another interesting feature occurs at $2\theta \approx 58^\circ$ [see Figs. 1(a)–1(d)], where the relative intensity of the double peak structure shows a change with increasing x . For the Nd series, the two peaks become equal in intensity for $x \geq 0.3$, see Fig. 1(d). This observation strongly suggests¹² that with increasing x ordering or disordering of oxygen occurs at chain sites in Nd based samples, which supports the previous observation. In comparison, for Er based samples, the relative intensity of the double peaks at $2\theta \approx 58^\circ$ is not affected much by increasing x [see Fig. 1(a)], reflecting not much change in the order-disorder at chain sites with x . Sm and Y samples show a similar behavior as that of Nd and Er based samples, respectively, which is consistent with the trends of the OD and c -parameter changes discussed above. Detailed structural comparisons of Ca substituted Er, Y, Sm, and Nd series will be presented elsewhere.

B. Iodometric titration

For all four Er, Y, Sm, and Nd sets of samples, the oxygen content, as determined by iodometric titration, is found to decrease with increasing x . This means that the Ca substi-

tution at the R site in Er, Y, Sm, and Nd:123 samples create oxygen vacancies. The oxygen content and the average Cu valence for all samples are given in Table I.

C. Resistivity, ac susceptibility, and superconducting critical temperature

In Figs. 2(a)–2(d), we plot the resistivity as a function of temperature for all the samples of series $R_{1-x}\text{Ca}_x\text{Ba}_2\text{Cu}_3\text{O}_{7-\delta}$ ($R=\text{Er, Y, Nd, and Sm}$ with $x=0.0$ to 0.50). The increase of the room temperature resistivity with increasing x endorses the substitution of Ca in the lattice. Interestingly, the $\rho(T)$ curves show distinct upward curvature for the Er/Y series of samples, while the same is absent in case of the Sm/Nd samples. The only exception is the $x=0.5$ Nd based sample. We remark here that since $x=0.5$ samples show impurity phases, the curvature shown by $x=0.5$ Nd based sample is to be taken only cautiously. A quick glance at Fig. 2 shows the depression in T_c with increasing x . It is remarkable to note that the relative decrease in $T_c(\rho=0)$ is more for Er and Y samples, when compared with those of Sm and Nd ones.

For all four series, the superconducting transitions were also measured by ac magnetic susceptibility. The behavior of diamagnetically observed shift in transitions with x corroborates well, in general, with the resistively measured transitions. Figure 3 depicts typical ac susceptibility transitions for the Y based samples. Clearly, the diamagnetic onset and the transition shifts to lower temperatures with increasing x . However, we observed a decrease in the screening fraction for all the samples with increasing x , which is presently unclear. We would like to comment here that small Meissner or screening fractions and their dependence on doping in

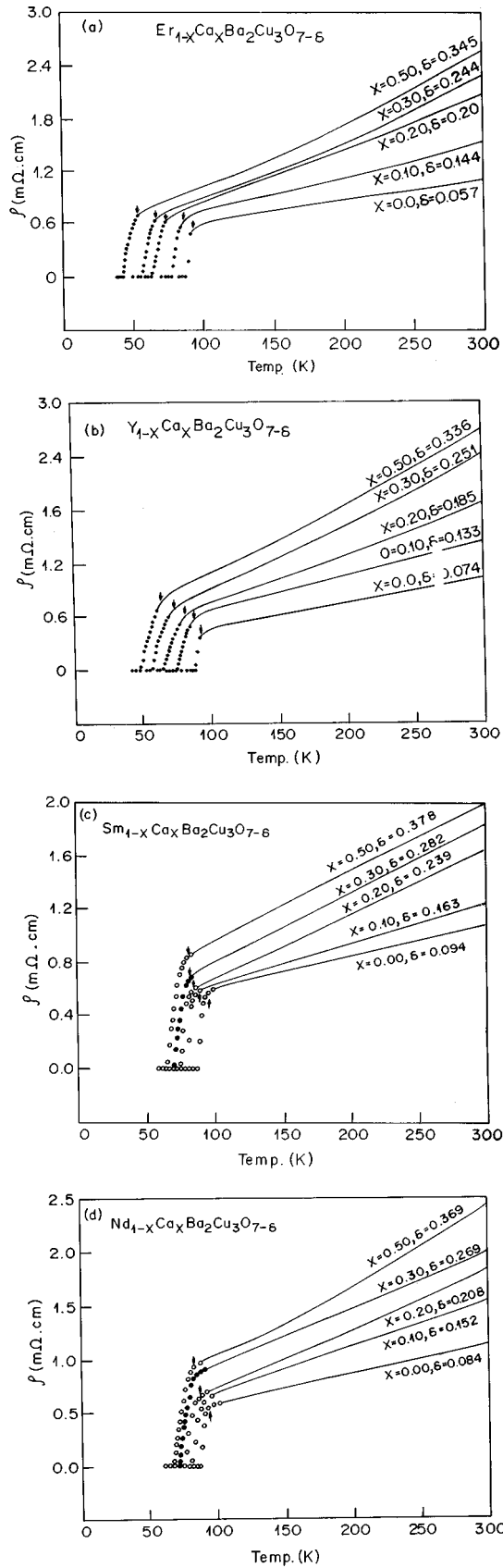


FIG. 2. Resistivity versus temperature plots for (a) $Er_{1-x}Ca_xBa_2Cu_3O_{7-\delta}$, (b) $Y_{1-x}Ca_xBa_2Cu_3O_{7-\delta}$, (c) $Sm_{1-x}Ca_xBa_2Cu_3O_{7-\delta}$, and (d) $Nd_{1-x}Ca_xBa_2Cu_3O_{7-\delta}$. The arrows in the figure mark the onset of the superconducting transition T_{on} .

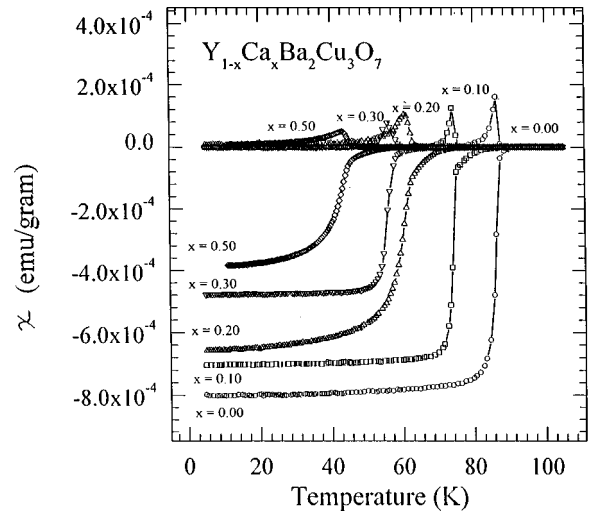


FIG. 3. ac susceptibility versus temperature plots for $Y_{1-x}Ca_xBa_2Cu_3O_{7-\delta}$.

HTSC's, has often been observed (e.g., see Refs. 10 and 13). This might reflect an inherent disorder or inhomogeneity in the multicomponent HTSC materials, and needs to be looked into more carefully in the future.

To show more explicitly the T_c dependence on x for all four series of samples, the $T_c(\rho=0)$ is plotted as a function of x in Fig. 4. As can be easily marked, the T_c change with x is steeper for Er/Y than in Sm/Nd samples. Notice also that the $T_c(x)$ tends to saturate in Sm/Nd samples, the origin of which is related with oxygen loss and will be discussed shortly. The saturation in T_c with x is nearly absent for the Er/Y series (see Fig. 4). To cross check that our samples represent the intrinsic behavior of the Ca substituted 1-2-3 compounds, we compare in Fig. 5 the $T_c(x)$ graphs of Er and Y with those cited earlier in the literature.^{2,4,5,8} The agreement is found to be good.

Since Ca substitution leads to a change in oxygen content for all the samples (see Sec. III B), we also plot their $T_c(\rho=0)$ as a function of oxygen content (δ) in Fig. 6. For comparison we have also included the well known $T_c(\delta)$ curve

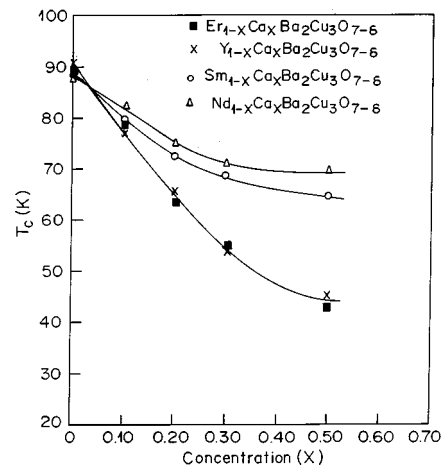


FIG. 4. $T_c(\rho=0)$ versus x (Ca concentration) for (a) $Er_{1-x}Ca_xBa_2Cu_3O_{7-\delta}$, (b) $Y_{1-x}Ca_xBa_2Cu_3O_{7-\delta}$, (c) $Sm_{1-x}Ca_xBa_2Cu_3O_{7-\delta}$, and (d) $Nd_{1-x}Ca_xBa_2Cu_3O_{7-\delta}$. The lines are only a guide to the eye.

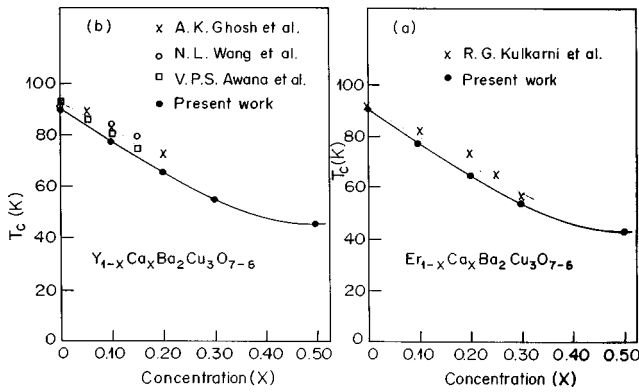


FIG. 5. Comparison of presently observed $T_c(x)$ variation with reported data for (a) $\text{Er}_{1-x}\text{Ca}_x\text{Ba}_2\text{Cu}_3\text{O}_{7-\delta}$ and (b) $\text{Y}_{1-x}\text{Ca}_x\text{Ba}_2\text{Cu}_3\text{O}_{7-\delta}$. The lines are only a guide to the eye.

for pure Y:123 (Ref. 13) in the same figure. As seen from the figure, the T_c decreases sharply without any saturation with increasing δ for Er and Y based samples. In contrast, the Nd and Sm based samples show a behavior which tends to mimic the pure Y:123 compound, i.e., the $T_c(\delta)$ after an initial decrease tends to show a plateau near $\delta=0.30$.

IV. DISCUSSION

The results of x-ray diffraction, iodometric titration, normal state resistivity, and T_c measurements can be summarized as follows.

(1) Ca substitutes isostructurally in Er, Y, Sm, and Nd based $R_{1-x}\text{Ca}_x:123$ samples, with only a small impurity phase(s) for $x=0.50$ in all four cases. The OD is only weakly effected for Er/Y, however, the same decreases faster with x for Sm/Nd samples. The c -lattice parameter in general increases with x , and the increase is much stronger for Sm/Nd samples. For $x \geq 0.3$, Er/Y based samples clearly show a transformation to the ortho II phase, as only traces of the same could be detected in the case of Sm/Nd samples.

(2) Ca substitution leads to a proportionately increasing loss of oxygen in all Er, Y, Sm, and Nd based samples. The average Cu valence slightly decreases (as compared to pure R:123), but stays nearly independent of x for all the series.

(3) The normal state $\rho(T)$ curves show curvature for Er/Y based samples, while the same is absent in case (except $x=0.5$ Nd:123) of Sm/Nd. The $T_c(\rho=0)$ decreases with x and δ for all the four set of samples, and the decrease is stronger in the case of Er/Y samples.

Now we demonstrate that all the above mentioned points consistently indicate an oxygen loss occurring from different sites in the Er/Y and Sm/Nd sets of samples. First we show how points 1 and 2, along with the ionic radii and coordination number considerations, suggest a different site preference for oxygen vacancies in different samples. In eightfold coordination the trivalent Er, Y, Sm, and Nd ions have radii of 1.00, 1.02, 1.09, and 1.12 Å, respectively. For divalent Ca, in eightfold coordination, the ionic radius is 1.12 Å. Clearly, in eightfold coordination, the ionic size of Ca^{2+} matches the sizes of Sm and Nd ions well, and is much bigger when compared to that of Er and Y ions. However, interestingly, the ionic size of sixfold coordinated Ca^{2+} (1.00 Å) matches that of the eightfold coordinated Er and Y ions well. This

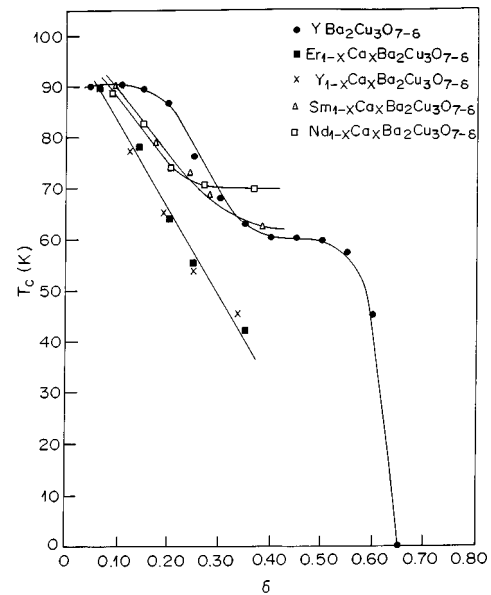


FIG. 6. $T_c(\rho=0)$ versus δ (oxygen content) for (a) $\text{Er}_{1-x}\text{Ca}_x\text{Ba}_2\text{Cu}_3\text{O}_{7-\delta}$, (b) $\text{Y}_{1-x}\text{Ca}_x\text{Ba}_2\text{Cu}_3\text{O}_{7-\delta}$, (c) $\text{Sm}_{1-x}\text{Ca}_x\text{Ba}_2\text{Cu}_3\text{O}_{7-\delta}$, and (d) $\text{Nd}_{1-x}\text{Ca}_x\text{Ba}_2\text{Cu}_3\text{O}_{7-\delta}$. The lines are only a guide to the eye.

indicates that for Sm and Nd based R:123, Ca on substitution can acquire the same coordination number of 8 as the R site. The loss of oxygen (point 2) in Sm and Nd samples can thus be accounted for by the loss from chain site O(1) oxygen. This is also supported by the decrease in OD (point 1) in Sm and Nd based samples. On the other hand, it seems highly probable that Ca substitutes in sixfold coordination at the site of eightfold coordinated Er and Y ions in the R:123 lattice. The sixfold coordinated Ca necessitates the creation of oxygen vacancies in the adjacent CuO_2 planes, which might be the case of Er and Y based samples to account for the oxygen loss. This is also in good agreement with the nearly invariant OD (point 1) in Er and Y samples, which reflects that the chain site oxygen O(1) is left relatively untouched. The creation of oxygen vacancies at CuO chain sites (CuO_2 plane sites) for Nd/Sm (Er/Y) is supported by the relative presence (absence) of ortho II phase (point 1), respectively.

Further evidence of oxygen loss from CuO_2 planes for Er/Y and from CuO chains in case of Sm/Nd is suggested by the normal state $\rho(T)$ behavior (point 3). Note that the average Cu valence (point 2) in the studied samples, although invariant with x , decreases slightly with respect to the pure ($x=0$) samples. Thus the curvature in $\rho(T)$ for Ca substituted Er and Y samples cannot be due to overdoping, and can be understood only by disorder induced localization. Considering that electrical transport essentially involves the CuO_2 planes, the $\rho(T)$ curvature is an indication of disorder in CuO_2 planes. In contrast, the Ca substituted Sm and Nd samples show no sign of curvature in $\rho(T)$, reflecting more ordered CuO_2 planes. The $x=0.5$ Nd sample showing a curvature is not clear, however, the presence of impurity phases in it, calls for a separate investigation.

The next piece of evidence that it might be the different site preference of the oxygen vacancies in the case of Sm/Nd as compared to Er/Y samples, is hinted from $T_c(x, \delta)$ behavior (point 3). The $T_c(\delta)$ graph for Ca substituted Sm/Nd

samples was shown (see Fig. 6) to follow qualitatively the $T_c(\delta)$ graph of pure Y:123. The latter is understood¹⁴ in terms of the oxygen vacancy creation and ordering in CuO chains of the R :123 lattice, and by analogy may hold for Sm/Nd samples as well. The observed plateau in $T_c(\delta)$ of Sm/Nd, for $x \geq 0.3$, is in line with the transformation to ortho II phase seen by x rays (point 1), and well known for oxygen deficient pure Y:123 material. In clear contrast, the $T_c(\delta)$ of Ca substituted Er/Y samples shows a steeper slope and no plateau. This behavior does not fit with the known (pure Y:123) CuO chains scenario, which suggests the creation of oxygen vacancies elsewhere ("CuO₂ planes") in the unit cell for Er/Y samples. Also note that, for $x \geq 0.3$, in these two series only traces of ortho II phase (point 1) could be detected, which supports the near absence of plateau in $T_c(\delta)$.

Finally, we would like to say something more about the $\rho(T)$ behavior of all four sets of samples. We observe that the onset of the superconducting transitions (T_{on} , marked by arrows in Figs. 2(a)–2(d)] as a function of x shifts maximum for the Er based samples and minimum for the Nd based samples. This observation appears to be more than a coincidence, as we illustrate now. At the moment, admittedly, the mechanism by which the oxygen disordering of CuO chains can lead to a decrease of T_{on} , is not very clear. However, decreasing the conductivity of the chains by increasing the disorder is expected to broaden the $\rho(T)$ transition width without effecting the onset T_{on} .^{15,16} On the other hand, disorder in CuO₂ planes should lead to a direct suppression of the superconducting transition,^{15,16} i.e., T_{on} should also shift to lower T . Note that Er and Nd represent the extremes of the R (=Er, Y, Sm, Nd) series in terms of their ionic radii 1.00 and 1.12 Å, which match perfectly with sixfold and eightfold coordinated Ca²⁺, respectively. Therefore, ideally, we expect the loss of oxygen purely from the CuO₂ planes (CuO chains) for the end members Er (Nd), whereas for samples based on middle members Y (Sm) the oxygen loss may partially also occur from the CuO chains (CuO₂ planes). For Nd based samples [see Fig. 2(d)] the near absence of the shift in T_{on} and at the same time the shift in $T_c(\rho=0)$ to lower T with increasing x , is consistent with the disorder in chains. On the other hand, for Er based samples [see Fig. 2(a)], a clear strong shift in T_{on} with increasing x is consistent with the disorder in planes. Also, it is worth noting that the more pronounced curvature of $\rho(T)$ in Er based samples, as ex-

pected for Er being at the end of the R series, reflects more disorder in the CuO₂ planes.

V. CONCLUSIONS

We investigated the structural and superconducting properties of the $R_{1-x}\text{Ca}_x\text{Ba}_2\text{Cu}_3\text{O}_{7-\delta}$ system, with $R = \text{Er}, \text{Y}, \text{Nd},$ and Sm , and for $0.50 \geq x \geq 0.00$. We have shown that substitution of divalent Ca leads to a loss of oxygen in all the samples irrespective of the chosen R in R :123 system. The loss of oxygen compensates for the extra hole contribution due to Ca²⁺/ R ³⁺ aliovalence, resulting in an average Cu valence nearly independent of x for all R . The variation of orthorhombic distortion, c lattice parameter, and $\rho(T)$ with x , and the $T_c(x, \delta)$ behavior is significantly different in Er and Y with respect to Sm and Nd based R :123 systems. We suggest and provide evidence that these differences are a consequence of different structural order or disorder of oxygen vacancies created by Ca substitution. Presumably, the oxygen loss occurs predominantly in CuO₂ planes for Er/Y based samples and in CuO chains for Sm/Nd based samples.

Finally, we would like to comment on certain reports^{9,10} where the decrease in T_c of the optimally oxygenated $\text{Y}_{1-x}\text{Ca}_x$:123 samples has been solely attributed to the over-doping due to Ca²⁺/ Y ³⁺ aliovalence. However, there are clear pitfalls in the results of^{9,10} (1) the use of a single $T_{c,\text{max}}$ for normalization in Fig. 2 of Ref. 9 is incorrect, since as shown in the inset of Fig. 1 of Ref. 9 the value of $T_{c,\text{max}}$ depends on the amount of substituted Ca; (2) for a change of $T_c/T_{c,\text{max}}$ from 1 to 0.6, the corresponding change of hole concentration differs by a factor 3 in Refs. 9 and 10. We believe, these discrepancies cannot be understood without taking into account the disorder due to oxygen vacancies in the $\text{Y}_{1-x}\text{Ca}_x$:123 system.

The present study highlights the effect of oxygen vacancies on the superconductivity of the R :123 system, which are more detrimental when created in the CuO₂ planes as compared to CuO chains. Our work emphasizes the need of paying more attention to the local structural disorder in HTSC's and its impact on superconductivity.

ACKNOWLEDGMENTS

The authors thank Professor S. K. Joshi for his continued interest.

¹A. Manthiram and J. B. Goodenough, *Physica C* **159**, 760 (1989).

²N. L. Wang, M. C. Tan, J. S. Wang, S. Y. Zhang, H. B. Jiang, J. Sha, and Q. R. Zhang, *Supercond. Sci. Technol.* **4**, S307 (1991).

³B. Fisher, G. Genossar, C. G. Kuper, L. Patlagan, G. M. Reisner, and A. Knizhnik, *Phys. Rev. B* **47**, 6054 (1993).

⁴R. G. Kulkarni, R. L. Raibagkar, G. K. Bichile, A. Shaikh, J. A. Bhalodia, G. J. Baidha, and D. G. Kuberkar, *Supercond. Sci. Technol.* **6**, 678 (1993).

⁵V. P. S. Awana and A. V. Narlikar, *Phys. Rev. B* **49**, 6353 (1994).

⁶V. P. S. Awana, A. Tulapurkar, S. K. Malik, and A. V. Narlikar, *Phys. Rev. B* **50**, 594 (1994).

⁷A. G. Kontos, R. Dupree, and Z. P. Han, *Physica C* **247**, 1 (1995).

⁸A. K. Ghosh, S. K. Bandhopadhyay, P. Barat, P. Sen, and A. N. Basu, *Physica C* **264**, 255 (1996).

⁹J. L. Tallon, C. Bernhard, H. Shaked, R. L. Hitterman, and J. D. Jorgensen, *Phys. Rev. B* **51**, 12 911 (1995).

¹⁰G. Bottger, I. Magelschots, E. Kaldis, P. Fischer, Ch. Kruger, and F. Fauth, *J. Phys.: Condens. Matter* **8**, 8895 (1996).

¹¹W. E. Farneth, R. K. Bordia, E. M. McCarron III, M. K. Crawford, and R. B. Flippen, *Solid State Commun.* **66**, 953 (1988).

¹²V. S. Melnikov, V. M. Pan, and A. V. Zhalko-Titarenko, in *Studies of High Temperature Superconductors*, edited by A. V. Narlikar (Nova, Commack, NY, 1991), Vol. 7, p. 266.

- ¹³R. J. Cava, B. Batlogg, K. M. Rabe, E. A. Rietman, P. K. Gallagher, and L. W. Rupp, Jr., *Physica C* **156**, 523 (1988).
- ¹⁴J. D. Jorgensen, *Phys. Today* **44** (6), 34 (1991).
- ¹⁵A. V. Narlikar, P. K. Dutta, S. B. Samanta, and V. P. S. Awana, in *Studies of High Temperature Superconductors*, edited by A. V. Narlikar (Nova, Commack, NY, 1991), Vol. 10, p. 1.
- ¹⁶A. K. Bandyopadhyay, D. Varandani, E. Gmelin, and A. V. Narlikar, *Phys. Rev. B* **50**, 462 (1994).